Effect of Ring Rigidity on the Statics and Dynamics of Linear Catenanes

Macromolecules

pubs.acs.org/Macromolecules Article

Effect of Ring Rigidity on the Statics and Dynamics of Linear Catenanes

Pietro Chiarantoni and Cristian Micheletti*

Cite This: https://doi.org/10.1021/acs.macromol.1c02542 Read Online

ACCESS | Metrics & More | Article Recommendations | Supporting Information

ABSTRACT: We used molecular dynamics simulations to investigate the statics and dynamics of poly[n]catenanes for different bending rigidities of the constituent rings. We show that stiffer rings yield catenanes with more extended and, at the same time, more flexible backbones. The softening of the backbone reflects the decreasing steric interactions of catenated rings as their shape becomes more oblate due to increased rigidity. The internal dynamics of catenanes is affected too. Going from flexible to rigid rings causes a several-fold slowing of different processes, from segmental rotations and size fluctuations to Rouse modes. Finally, by considering the statics and dynamics of crowded solutions of catenanes, we isolate another emergent property controlled by the rigidity of the rings. Specifically, we show that catenanes with rigid rings hinder each other's motion more than those with flexible rings. Thus, in equally crowded solutions, the diffusion coefficient is smaller for catenanes with stiffer rings.

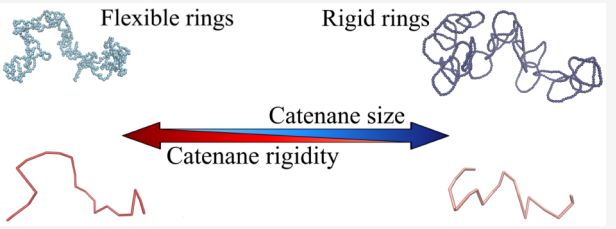

INTRODUCTION

Supramolecular constructs formed by entangled molecules are increasingly studied for their relevance in a broad range of contexts, such as living cells, soft matter systems, and synthetic meta-materials.[1−15] For instance, the intertwining of linear polymer chains is the distinctive feature of domain-swapped protein assemblies,[16,17] it defines the rheological and mechanical properties of dense polymer solutions,[18−24] and it is harnessed to stabilize self-assembled meta-materials.[25−29]

Perhaps the most intriguing forms of molecular intertwining are offered by extended systems made of interlocked ring polymers. Notable examples include networks of linked DNA rings, both natural[12,30−33] and artificial,[34,35] and non-DNA based topological materials,[29,36−41] molecular motors, and molecular electronics.[7,42]

In all such systems, the interlockings of molecules with a closed covalently bonded backbone have been aptly named "mechanical bonds", a term that simultaneously conveys the permanent character of the intermolecular topological constraint as well as the more tolerant distance fluctuations afforded by the linking constraint compared to covalent bonding.

Linear catenanes, or poly[n]catenanes, are the simplest systems where the emergent properties of mechanical bonding can be addressed and contrasted with those of conventionally bonded linear polymers.[4,6,43] Starting from the seminal study of ref40, where linear catenanes of up to 27 macrocycles were successfully synthesized, several efforts have been spent in this direction. We now know how catenanes respond to mechanical stretching,[24,40] how their relaxation dynamics in isolation or in solution varies at different scales,[44−46] and how metric scaling is defined by the interplay of the size and number of linked rings.[47−49]

Despite these advancements, key questions about the emergent properties of linear catenanes remain open. In particular, the effects of the macrocycles bending rigidity on the static and dynamics of linear catenanes are still largely unknown.

Motivated by these considerations, here we present a first systematic study of the statics and dynamics of linear catenanes, both in isolation and in solutions, formed by interlocked rings of varying size and bending rigidity. We consider extensive sets of configurations obtained from Langevin dynamics simulations and carry out a comparative multiscale analysis of various metric and dynamical properties.

By isolating the effects of mechanical bonding and structural rigidity we identify novel emergent properties. We show that increasing ring rigidity yields catenanes whose backbone has a larger metric size but is also more flexible. In addition, various internal dynamical processes, from segmental relaxation to Rouse modes, are progressively slowed down by the stiffening of the interlocked rings. Finally, the diffusion coefficient in crowded solutions is shown to decrease too. By using a

Received: December 14, 2021
Revised: March 18, 2022

https://doi.org/10.1021/acs.macromol.1c02542
Macromolecules XXXX, XXX, XXX−XXX

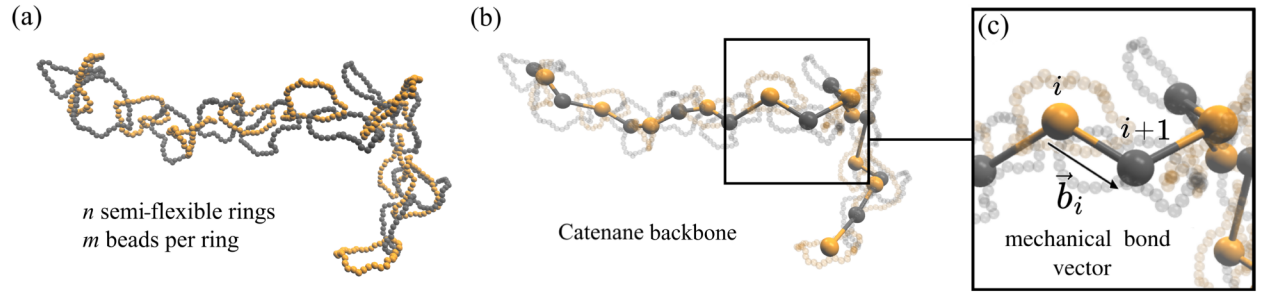

Figure 1. Model catenane, effective backbone and mechanical bonds. (a) Typical configuration of a model poly[n]catenane of n = 20 rings, each with m = 40 monomers and with bending rigidity $\kappa_b = 5\epsilon$. (b) The statics and dynamics analysis was mostly based on the catenane effective backbone, the virtual linear chain connecting the centers of mass (CoMs) of the rings. (c) The vector connecting the CoMs of two consecutive rings, i and $i + 1$ defines the corresponding mechanical bond, $\vec{b}_i\vec{b}_i$. The decay of the mechanical bonds orientational correlation is used to establish the effective persistence length of the catenanes backbone, and thus the overall rigidity of the catenanes. In all panels, an alternating gray and orange coloring of the rings was used for visual clarity.

multiscale analysis, we provide a microscopic rationale for the above properties.

MODEL AND METHODS

Model Definition and Simulation Setup. We considered linear catenanes of n semiflexible rings, each ring being made of m monomers, see Figure 1a. A single poly[n]catenane thus comprises a total of $n \cdot m$ monomers of nominal diameter σ. A standard truncated and shifted Lennard-Jones potential is used for the excluded volume interaction of all pairs of monomers in the same or different rings,

$$U_{\mathrm{LJ}} = \begin{cases} 4\epsilon\left[\left(\frac{\sigma}{r}\right)^{12} - \left(\frac{\sigma}{r}\right)^{6} + \frac{1}{4}\right] & r \le r_c = 2^{1/6}\sigma \\ 0 & \text{otherwise,} \end{cases} \quad (1)$$

where r is the distance of the two monomers, and the characteristic energy scale ϵ is set equal to the system thermal energy, k_BT. In addition to U_{LJ}, consecutive monomers on the ring contour also interact via a bonding FENE potential,[19] which provides the backbone connectivity:

$$U_{\mathrm{FENE}} = \begin{cases} -0.5k_{\mathrm{FENE}}R_0^2\ln\left(1 - \left(\frac{r}{R_0}\right)^2\right) & r \le R_0 \\ \infty & r > R_0, \end{cases} \quad (2)$$

where $k_{\mathrm{FENE}} = 30\epsilon/\sigma^2$ and $R_0 = 1.5\sigma$.

The rings rigidity was set via a standard bending energy term for triplets of consecutive monomers, $\{i, i + 1, i + 2\}$, along the (periodic) ring contour,

$$U_{\mathrm{bend}} = \kappa_b(1 - \vec{u}_i\cdot\vec{u}_{i+1}), \quad (3)$$

where κ_b is the bending rigidity and $\vec{u}_i$ is the normalized (adimensional) bond vector of monomers i and $i + 1$.

Langevin dynamics simulations of the system were carried out with the LAMMPS[50] simulation package. The friction coefficient ζ was set as in ref19 and the integration time step was equal to $0.005\tau_{\mathrm{LJ}}$, where $\tau_{\mathrm{LJ}} = \sigma\sqrt{M/\epsilon}$ is the characteristic Lennard-Jones time and M is the monomer mass.

We first addressed isolated catenanes in a periodic cubic box. For any given combination of model parameters, see further below, we collected 10 independent trajectories of duration between 1.25×10^6 τ_{LJ} and $2 \times 10^7\tau_{\mathrm{LJ}}$. The initial configurations were obtained by relaxing a straight catenane arrangement over a timespan of $5 \times 10^5\tau_{\mathrm{LJ}}$, which is much larger than the system autocorrelation time. For the latter, we considered the orientation of the end-to-end vector, that is, the distance vector of the centers of mass of the first and last rings, which takes a maximum value of $6 \times 10^4\tau_{\mathrm{LJ}}$ among all structures and rigidities.

We also considered solutions of catenanes and collected 5 independent trajectories, each of duration $10^6\tau_{\mathrm{LJ}}$, at any considered value of κ_b. The initial configurations were obtained by relaxing a regularly spaced and nonoverlapping arrangement of compact catenanes, sampled from the fully flexible ($\kappa_b/\epsilon = 0$) ensemble.

Model Parameters. We considered isolated poly[n]catenanes of n = 20 rings with $m = \{10, 20, 40\}$ monomers each and varied the bending rigidity in the $0 \le \kappa_b/\epsilon \le 20$ range. The side of the periodic simulation box was set equal to 300σ, which is several-fold larger than the mean gyration radius of all simulated catenanes. Additionally, to study the effect of inter-ring interactions, we switched off the excluded volume interactions between monomers belonging to rings at sequence separation $|i - j|$ larger than $|i - j|_{\max} = 1, 2, 3$, and so forth, where i and j are the sequential indexes of the rings along the catenane.

For the solutions, we considered 27 catenanes with n = 20 and m = 40, for a total number of 21,600 monomers, and varied κ_b/ϵ in the 0.6−20 range. The side of the periodic box was set to $L = 85\sigma$.

Equivalent Linear Chain Model. To better study the effects of mechanical bonding, we compared the dynamics of catenanes with that of linear chains of equivalent overall size and mobility. The correspondence is informed by different criteria than used before[44] and maps a catenane of n rings of m monomers and rigidity κ_b onto a semiflexible linear chain of n equivalent monomers interacting via LJ, FENE, and bending rigidity potentials analogous to those of eqs 1−3.

Specifically, to match the static metric properties, the effective size of the equivalent monomers was set so as to match the mean squared (mechanical) bond length and the bending rigidity was next chosen to match the gyration radius of the catenanes backbone. To match the overall dynamical properties, the effective mass of the equivalent monomers and the effective friction coefficient were both set to be m times larger than for the monomers of the catenane rings. This mapping ensures that the CoMs of isolated catenanes and isolated equivalent linear chains have identical diffusivities and velocity autocorrelation times.

Catenane Backbone. Most of the analysis was carried out for the so-called linear image of the catenanes, that is their virtual backbone obtained by connecting the centers of mass of consecutive rings, see the sketch of Figure 1b. Linear images were used to compute salient global metric properties, such as the gyration radius and the end-to-end vector of a catenane, and more local ones related to the mechanical bond vectors, $\vec{b}$, that is, the vectors joining the CoMs of consecutive rings, see Figure 1c. As sketched in the same figure, we analyzed how the rings rigidity, κ_b, affects the length of mechanical bonds, b. We also computed the tangent−tangent correlation function of mechanical bonds at different separation s along the catenane, $C(s) = \langle\vec{b}_i\cdot\vec{b}_{i+s}/(|\vec{b}_i||\vec{b}_{i+s}|)\rangle$, where the average is taken over all

https://doi.org/10.1021/acs.macromol.1c02542
Macromolecules XXXX, XXX, XXX−XXX

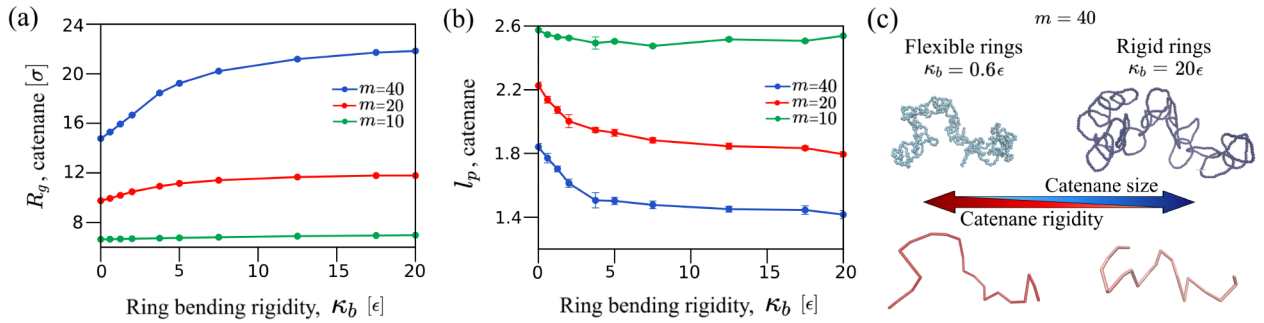

Figure 2. Stiffer rings yield more flexible and larger catenanes. (a) The root mean squared gyration radius, R_g, and (b) the persistence length, l_p, of the catenane backbone are shown as a function of the ring bending rigidity, κ_b. The three curves are for three different ring sizes, m = 10, 20, 40. Increasing the bending rigidity of the rings thus yields catenanes that are larger in size, but also more flexible, as graphically summarized in panel (c). In the upper part of the panel, two typical configurations for m = 40 at $\kappa_b = 0.6\epsilon$ and $\kappa_b = 20\epsilon$ are portrayed at the same scale. The different effective flexibility is conveyed by the different smoothness of the corresponding backbones that, for a more direct comparison, have been rescaled so that the average bond length is the same.

sampled configurations and by sliding the ring index i in the admissible range. The effective persistence length, l_p of the catenane was evaluated as the integral of $C(s)$ computed from $s = 0$ up to when $C(s)$ first falls below 10^{-2}. Notice that l_p, is dimensionless, as it describes the number of mechanical bonds over which the catenane backbone directionality decays. This appears to be the natural generalization of the usual definition of persistence length for covalently bonded chains, given that mechanical bonds do not have a fixed length.

Rings Size and Shape. To address the impact of mechanical bonding and structural rigidity on ring size and shape we considered the gyration tensor,

$$Q_{\alpha\beta} = \frac{1}{m}\sum_{i=1}^{m} r_i^{(\alpha)} r_i^{(\beta)} - \frac{1}{m^2}\sum_{j=1}^{m} r_j^{(\alpha)} \sum_{k=1}^{m} r_k^{(\beta)} \tag{4}$$

where, $r_i^{(\alpha)}$ is the α^{th} Cartesian coordinate of the i^{th} bead in a ring, and m is the number of beads per ring. We identified the eigenvectors, or principal directions, and the corresponding eigenvalues λ_α^2, customarily ranked in descending order, $\lambda_1^2 \geq \lambda_2^2 \geq \lambda_3^2$. The spectrum of Q was used to compute two shape parameters: the asphericity, Δ, and the nature of asphericity, Σ. Their definitions are as follows:[51]

$$\Delta = \frac{3}{2}\frac{\mathrm{Tr}\hat{Q}^2}{(\mathrm{Tr}Q)^2}, \tag{5}$$

$$\Sigma = \frac{4\det\hat{Q}}{\left(\frac{2}{3}\mathrm{Tr}\hat{Q}^2\right)^{3/2}}, \tag{6}$$

where $\hat{Q} = Q - \delta_{ij}\mathrm{Tr}Q/3$. The asphericity satisfies the inequality $0 \leq \Delta \leq 1$, with $\Delta = 0$ for a spherically symmetric object and $\Delta = 1$ for a rigid rod. The nature of asphericity instead ranges from -1 to 1, with negative and positive values indicating oblate and prolate shapes, respectively, while the modulus quantifies the oblateness/prolateness degree. A planar circle corresponds to $\Delta = 1/4$ and $\Sigma = -1$.

The same definition of the gyration tensor, but computed for the backbone coordinates, was used to characterize the size and shape of catenanes.

Direct Analysis of Catenanes Segmental Dynamics. To characterize the global relaxation of isolated chains, we considered the autocorrelation functions for the squared gyration radius and of the end-to-end vector orientation,[52] which we integrated to obtain the corresponding time scales, $\tau_{R_g^2}$ and τ_{rot} for backbone segments of varying length $|i - j|$. The segments were taken with the midpoint in the center of the catenane and symmetrically extended along the contour to minimize chain ends effects. The same quantities were computed for equivalent linear chains too.

The κ_b-dependent mobility of interacting catenanes in solutions was characterized via the mean squared displacement of the catenanes' centers of mass.

Rouse Mode Analysis. We performed a Rouse mode analysis of the dynamics both for catenanes backbone and for the equivalent chains. The Rouse modes of a given backbone conformation are defined as[53]

$$\vec{X}_p(t) = \frac{1}{n}\sum_{i=1}^{n} \vec{R}_i(t)\cos\left[\frac{p\pi}{n}\left(i - \frac{1}{2}\right)\right] \tag{7}$$

where $\vec{R}_i(t)$ is the coordinate vector of the i^{th} site of the catenane backbone at time t. In the above expression, $p = 0\cdots(n-1)$ is the index of the mode and the associated wavelength is n/p. The $p = 0$ mode, associated with the motion of the backbone CoM, was not considered. The characteristic relaxation time of the p^{th} mode, τ_p, is given by,

$$\tau_p = \int_0^\infty C(p,\tau)\,\mathrm{d}\tau \tag{8}$$

where $C(p,\tau) = \langle \vec{X}_p(t+\tau)\cdot\vec{X}_p(t)\rangle / \langle \vec{X}_p(t)\cdot\vec{X}_p(t)\rangle$ is the mode correlation function, and $\langle\rangle$ denotes the average over time, t. For the numerical evaluation of the integral, τ was varied from 0 up to when $C(\tau)$ first falls below 10^{-2}.

The viability of the Rouse mode analysis for catenanes with different ring rigidities was assessed by testing the Gaussianity and statistical independence of the distributions of the modes amplitudes.[44]

RESULTS

Statics of Isolated Catenanes. We first considered isolated catenanes of n = 20 rings, each of $m = \{10, 20, 40\}$ monomers. We analyzed the static properties of the catenanes backbone as the rings bending rigidity, κ_b/ϵ, was systematically varied in the 0−20 range.

The results, summarized in Figure 2, present two contrasting properties. First, the mean gyration radius of the catenanes backbone, R_g, increases with the rings bending rigidity. The monotonic increase is observed at all rings sizes and is more prominent for the largest considered rings, m = 40. Second, the persistence length, l_p, of the catenane backbone is found to *decrease* with the rings rigidity. Again, this effect is observed at all values of m, though is largest for m = 40. Notice that l_p is dimensionless and measures the number of consecutive linked rings or, equivalently, of mechanical bonds, over which the

https://doi.org/10.1021/acs.macromol.1c02542
Macromolecules XXXX, XXX, XXX−XXX

orientation of the catenane backbone is correlated, see Methods.

The data of Figure 2 thus establish the first main result of our study, namely that the progressive stiffening of the rings yields catenanes that are larger in size, but also softer. The effect, recapitulated in the sketch of Figure 2c, is an emergent property of mechanically bonded chains, since it has no analog in covalently bonded ones, where backbone stiffness and size go in parallel.

To investigate the microscopic origin of the effect, we probed the conformational properties of catenanes at different scales, both directly and by varying the inter-ring interactions.

We started by considering the impact of κ_b on the effective length, b, of the mechanical bonds. We recall that the latter are the vectors joining the CoMs of consecutive rings, see Figure 1c.

Figure 3a shows the probability distributions of b for rings of $m = 40$ at three values of the bending rigidity. When the latter increases, the distributions progressively shift to larger values: raising κ_b/ϵ from 0.6 to 20 causes a 50% increase of the average value of b, from 4.99σ to 7.51σ. This increase of the effective spacing of rings with κ_b is clearly an important contributor to the observed increase of R_g.

The width of the distributions increases with κ_b too, indicating that stiffer linked rings have larger excursions of their distances. This matches the expectation that the wiggle room of two linked rings is largest when these are planar circles, that is, for large κ_b. By the same token, one may expect that the relative positional and rotational freedom of two linked rings would be larger in the same limit, which could explain the observed softening of the catenanes backbone with growing κ_b.

Although intuitive and appealing, this explanation is not supported by a more detailed analysis of the data and the properties of catenanes, as we now discuss.

We first consider the distributions of the mechanical bond length rescaled by its mean value, $b/\langle b\rangle$. With such regularisation, all three probability distributions of Figure 3a appear to collapse on the same master curve, as shown in the inset. Thus, flexible and rigid linked rings have about the same wiggle room relative to their average separation. Equivalently, the relative fluctuations of mechanical bonds do not vary significantly from flexible to rigid rings. On the basis of this, it appears unlikely that considerations based solely on pairs of mechanically bonded rings can illuminate the observed softening of the catenane backbone.

To directly verify this, we modified the potential energy of the catenanes by keeping inter-ring excluded volume interactions only for pairs of rings, i and j, at maximum sequence separation $|i - j|_{max} = 1$, that is, consecutive rings. All other pairs of rings were treated as phantom. Such modification preserves the mechanical bonding, or connectivity of the catenane, but not necessarily its topology, as nonconsecutive rings can intersect. Repeating the tangent−tangent correlation analysis on the linear image of the modified catenanes yields the l_p vs κ_b curve shown in black in the lower part of Figure 3b. Consistent with the above considerations, l_p is now approximately constant and, remarkably, is at least five times smaller than the persistence length observed for the fully interacting catenane case, indicated by the ochre curve on top of Figure 3b. This indicates that, perhaps counter to intuition, the intertwining of mechanically bonded rings is not the key determinant of the catenane backbone rigidity. The latter, as

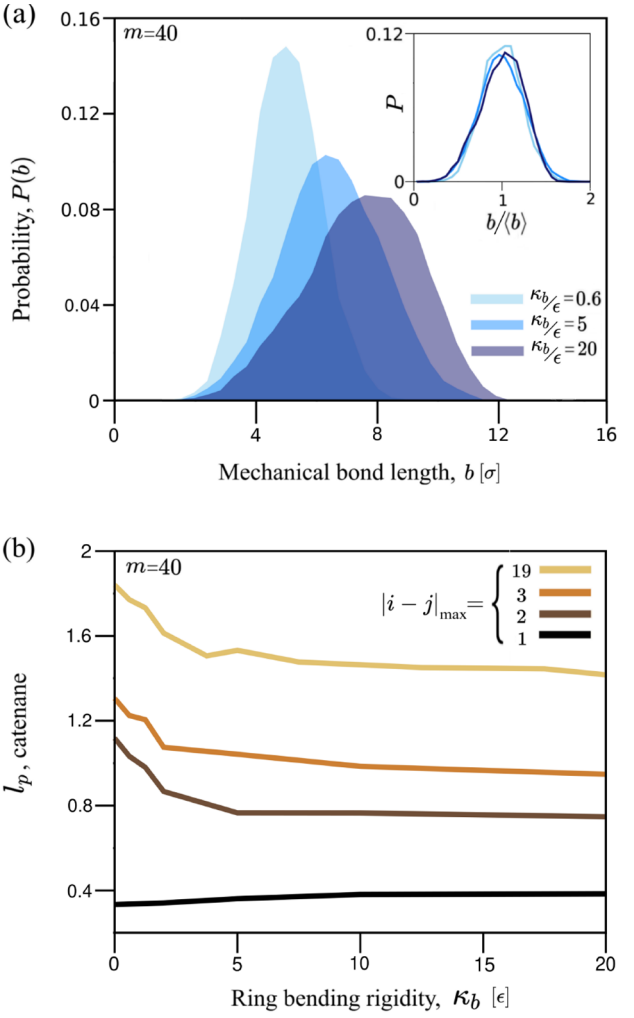

Figure 3. Microscopic origin of backbone rigidity. (a) The probability distributions of mechanical bond lengths, b, are shown for three different values of the ring bending rigity, κ_b. Data are for catenanes with rings of $m = 40$ beads. When the bond length is rescaled by the (κ_b-dependent) average value, the three curves collapse, see inset. This suggests that bonds fluctuations play a secondary role in the change of the flexibilty of catenanes. (b) The κ_b-dependence of the backbone persistence length, l_p, is shown for the original catenane model and for three different variants. In these variants, excluded volume interactions are switched off between monomers belonging to pairs of rings i and j with sequence separation $|i - j|$ larger than the indicated values. l_p is expressed in numbers of mechanical bonds, and thus is dimensionless.

we ascertained, is instead mostly established by excluded volume interactions of rings at larger sequence separations. This is illustrated by the brown and orange l_p curves in the middle of Figure 3b, which were obtained by retaining the excluded volume interactions up to sequence separations $|i - j|_{max} = 2$ and 3, respectively.

One notes that interactions for $|i - j|_{max} \leq 3$ already account for more than 50% to the total l_p, which clarifies that catenane rigidity is mostly defined by excluded volume interactions of nearby rings. The softening of the backbone for increasing κ_b thus reflects a diminished steric repulsion of concatenated rings that, as discussed further below, is brought about by changes of their shape.

https://doi.org/10.1021/acs.macromol.1c02542
Macromolecules XXXX, XXX, XXX−XXX

Importantly, the mechanical bond length, b, and the catenane persistence length, l_p, appear sufficient to recapitulate with good accuracy the multiscale metric properties of catenanes across all considered ring sizes and rigidities. To this end, we considered all backbone segments of different length, and plotted their rescaled gyration radii, $R_g/(\langle b\rangle \cdot l_p)$, versus the rescaled length, $|i-j|/l_p$. The rescaled data points, shown in Figure 4, all collapse onto a single curve, confirming that the softening of the catenanes backbone with κ_b occurs consistently across different segment lengths and ring sizes.

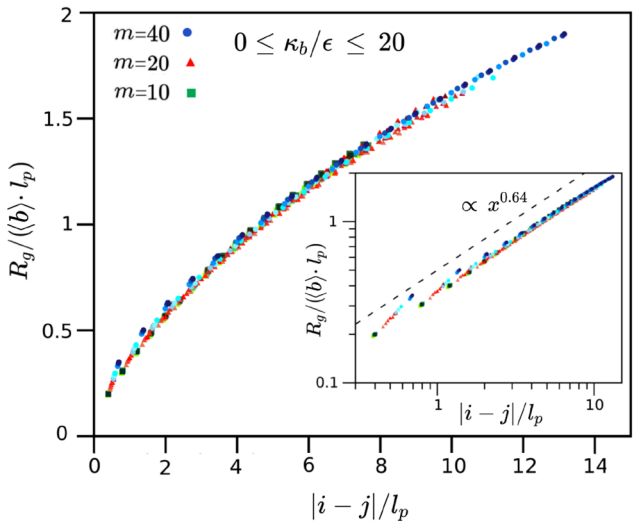

Figure 4. Metric scaling of backbone segments for different ring size and rigidities. The data show how the gyration radius, R_g, of backbone segments depend on segment length. The data points are for catenanes with different ring size, m and rigidity, κ_b. After rescaling by the appropriate "mechanical persistence length", which depends on both m and l_p as in Figure 2, the data collapse on a single curve. As shown in the inset, the scaling is compatible with an effective metric scaling exponent of $\nu \sim 0.64$, similar to the value reported in refs 47,49 for catenanes of comparable ring size and number. Unscaled data are provided in Figure S1.

Effect of Rigidity and Mechanical Bonding on Rings Size and Shape. To elucidate the microscopic basis of the κ_b-dependence of the self-hindrance of catenanes, we considered various geometric observables apt to characterize the average ring shape, namely: gyration radius, asphericity (Δ), and the so-called nature of asphericity parameter (Σ), see the Methods section. Further, to highlight the specific contributions of mechanical bonding, the same quantities were calculated for isolated rings.

The results are presented in Figure 5 and in Table S1 of the Supporting Information (SI), and allow to draw the following conclusions. First, increasing κ_b yields a substantial growth of the overall ring size, R_g, which nearly doubles from the fully flexible to the rigid case. Interestingly, mechanical bonding makes only a modest contribution to ring size, causing it to increase by at most 15%.

Mechanical bonding, however, has a major effect on ring shape at small rigidities, as it makes catenated rings much less prolate than in isolation. Notice, in fact, that for $\kappa_b/\epsilon \le 6$, the average values Σ varies from about 0.4 for isolated rings, indicative of substantial prolateness,[51] to about 0.1. The reduced prolateness results from the fact that catenated rings are entropically pulled in different directions by the mechanically bonded neighbors, and this pulling produces a less anisotropic shape than in isolation. This is confirmed by the data of shape anisotropy that, at all κ_b's, are smaller than for isolated rings.

From the vis-a-vis analysis of Δ and Σ, one concludes that upon increasing κ_b catenated rings, like isolated ones,[51] change the nature of their shape from a crumpled and (slightly) prolate three-dimensional structure, to an oblate one. For m = 40 the crossover occurs at $\kappa_b/\epsilon \sim 6$, where Σ changes sign and Δ is maximum. Notice that the $\kappa_b/\epsilon \sim 6$ is the also the rigidity beyond which l_p is only modestly affected by further changes of κ_b, see Figure 2b. From the above results, we conclude that the κ_b-dependent modulation of l_p due to intracatenane steric interactions reflects shape changes of catenated rings.

Orientational Order of Rings along Catenanes. We conclude the static analysis by discussing the average orientational order of two rings at different sequence distances, see Figure 6. As order parameter we considered $|\hat{n}_i \cdot \hat{n}_j|$, the scalar product (in modulus) of the normals to the principal planes of the rings i and j, the principal plane being defined by the two principal axes of the gyration tensor.

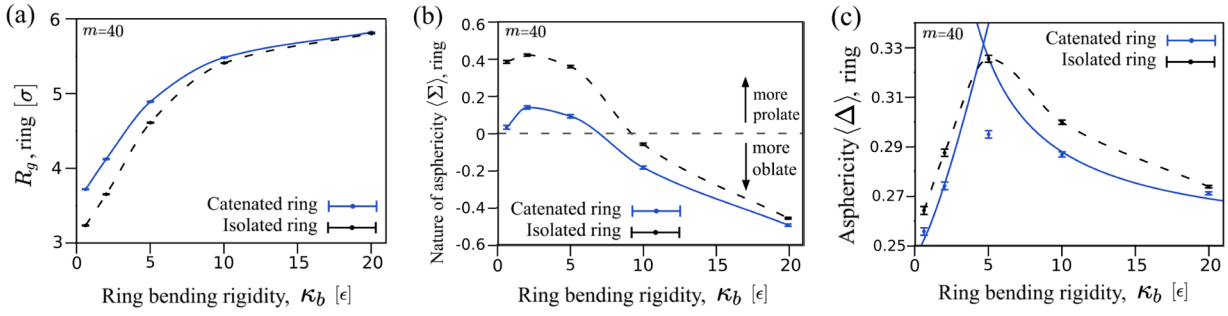

Figure 5. Effect of structural rigidity and mechanical bonding on ring size and shape. Panels (a), (b), and (c) show, respectively, the κ_b dependence of the gyration radius, R_g, nature of asphericity, Σ, and asphericity parameter, Δ, for rings of m = 40 beads in poly[20]catenanes. The two intersecting curves in panel (c) are best fits to the data points based on the asymptotic properties of isolated ring polymers:[51] $\Delta = 1/4 + a\cdot\kappa_b^{1.3}$ at small κ_b and $\Delta = 1/4 + a\cdot\kappa_b^{-1}$ at large κ_b, a being the fitting parameter. To highlight the role of mechanical bonding, the κ_b-dependence of R_g, Σ and Δ are shown for nonconcatenated rings of m = 40 beads, too. The data indicate that, as κ_b is increased, concatenated rings become larger and at $\kappa_b \sim 6\epsilon$ their conformation changes from slightly prolate to oblate. Further, mechanical bonding significantly reduces ring prolateness compared to the isolated case.

https://doi.org/10.1021/acs.macromol.1c02542
Macromolecules XXXX, XXX, XXX−XXX

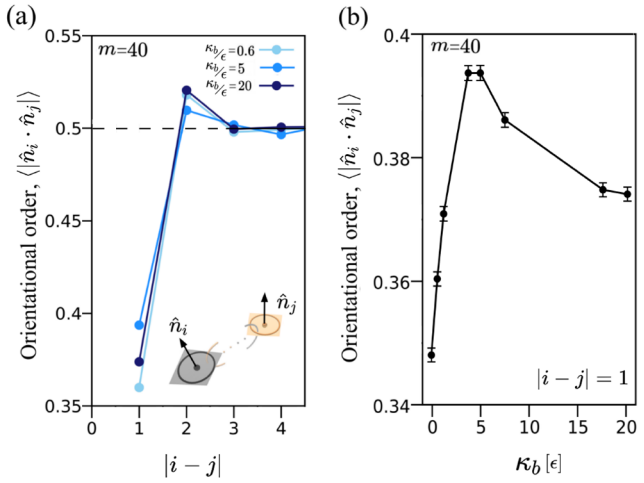

Figure 6. Ring orientational order along the backbone. (a) Average scalar product (in modulus) of the vectors normal to the principal planes of rings at various sequence distance, $|i - j|$. The data are for catenanes with rings of $m = 40$ beads and different rigidity. The horizontal dashed line at 1/2 marks the value expected for no orientational order. The data indicate a tendency to orthogonality of consecutive rings, $|i - j| = 1$. The orientational order of the latter is nonmonotonic with κ_b, as shown in panel (b), the peak value being at $\kappa_b \sim 6\epsilon$. The probability distributions for the orientational order parameters are provided in Figure S5.

For mechanically bonded rings, $|i - j| = 1$, the order parameter is smaller than 1/2 that, together with the skewed probability distribution (Figure S5a,d), points to a bias for orthogonal orientations. Interestingly, the strength of the bias is nonmonotonic with κ_b and, like the asphericity parameter, is maximum at $\kappa_b/\epsilon \sim 6$, see panel (b). The alternating orthogonal bias of consecutive rings, yields the observed modest degree of coplanarity (order parameter >1/2) at $|i - j| = 2$. The orientational order dissipates with increasing separation and is practically negligible for $|i - j| \geq 3$, when the order parameter (∼1/2) and the flatness of the probability distribution (Figure S5c,f) are consistent with a random relative orientation.

Dynamics of Isolated Catenanes. We next addressed the effect of the rings bending rigidity on the internal dynamics of catenanes, starting with the relaxation dynamics of segments of increasing length $|i - j|$ at or near the middle of the chain/catenane. For any segment length, we considered two different processes, the end-to-end vector reorientation and mean squared size fluctuations, whose characteristic times we indicate as τ_{rot} and $\tau_{R_g^2}$, respectively. In addition, we considered the relaxation times, τ_{Rouse}, of Rouse modes of different wavelength n/p, p being the Rouse mode index.

The data are given in the log−log plots of Figure 7 (Table 1), see Figure S6 for linearly scaled versions. The main result is that at any given length scale, all three dynamical processes are systematically slower for catenanes with rigid rings compared to fully flexible rings. For large segment lengths, $|i - j| \geq 14$, both τ_{rot} and $\tau_{R_g^2}$ at $\kappa_b/\epsilon = 20$ are three times larger than at $\kappa_b/\epsilon = 0$. This relative difference is approximately maintained at all segments lengths for $\tau_{R_g^2}$, while it reduces to 50% for τ_{rot} at $|i - j| = 1$. For Rouse times, the slowing down is about equal to 2.6 for all wavelengths.

The data in Figure 7 further clarify that, while $\tau_{R_g^2}$ and τ_{Rouse} remain comparable as the corresponding length scales are decreased, there is a growing gap with segmental reorientation times, τ_{rot}. As a matter of fact, τ_{rot} varies by only a factor of 3 across all segment lengths, while the other two time scales vary by more than 2 orders of magnitude. The rotational time thus emerges as the slowest relaxation process. This is because the rotational times of even short segments is strongly coupled to the rotation on the entire catenane. Consistent with this, no appreciable differences of τ_{rot} are seen with equivalent linear chains (continuous curves in Figure 7), while analogous data for $\tau_{R_g^2}$ and τ_{Rouse} confirm the general slowing-down introduced by mechanical bonds on more local processes and short length scales.[44]

We conclude by noting that κ_b also affects how well Rouse modes can describe the actual dynamics of the catenanes.

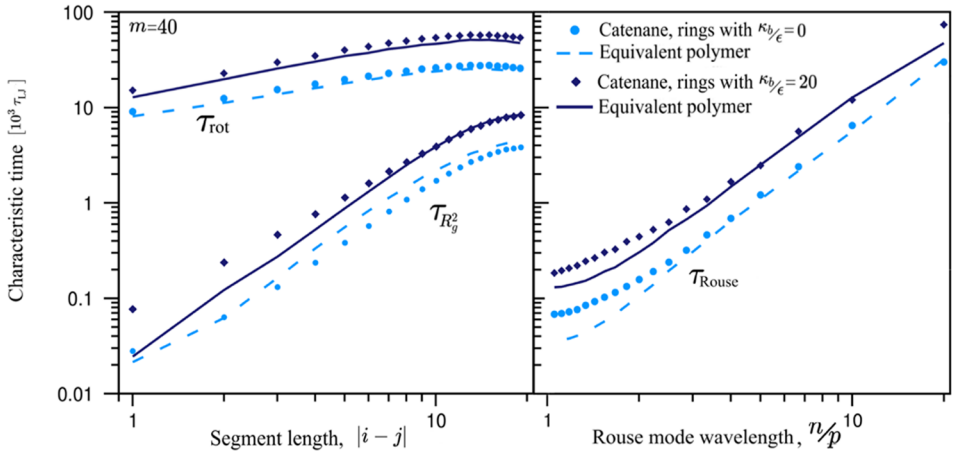

Figure 7. Catenane internal dynamics. The left panel illustrates the characteristic times of rotation and size fluctuations of backbone segments of varying length, $1 \leq |i - j| \leq 19$, of catenanes with either flexible or rigid rings. The right panel presents the characteristic times of Rouse modes of different wavelength, n/p, where $n = 20$ and $p = 1, ..., 19$ is the mode index. To highlight the effects of mechanical bonding, the same dynamical quantities are shown for suitably parametrized equivalent linear chains, see Table 1. The results, which are shown in linear scale in Figure S6, establish that increasing bending rigidity causes a several-fold slowing down of all considered dynamical processes.

https://doi.org/10.1021/acs.macromol.1c02542
Macromolecules XXXX, XXX, XXX−XXX

Table 1. Parametrization of Equivalent Linear Polymers[a]

catenane				equivalent chain						
20 rings of m = 40 monomers				20 effective monomers						
κ_b/ϵ	$\langle b^2\rangle/\sigma^2$	$\langle R_g^2\rangle/\sigma^2$	τ_{diff}/τ_{LJ}	$\tilde{\sigma}/\sigma$	$\tilde{\kappa}_b/\epsilon$	$\tilde{M}/M$	$\tilde{\zeta}/\zeta$	$\langle \tilde{b}^2\rangle/\sigma^2$	$\langle \tilde{R}_g^2\rangle/\sigma^2$	$\tilde{\tau}_{diff}/\tau_{LJ}$
0	23.21 ± 0.16	209.9 ± 1.11	14.03 ± 0.21	4.97	1.05	40	40	23.29 ± 0.06	210.0 ± 1.02	14.06 ± 0.31
20	59.66 ± 0.23	454.0 ± 5.71	30.06 ± 0.63	7.96	0.05	40	40	59.76 ± 0.03	456.0 ± 1.38	29.84 ± 1.81

[a]Parametrization of linear chains equivalent to catenanes with two different ring bending rigidities, $\kappa_b/\epsilon = \{0, 20\}$. The equivalent linear chains have 20 effective monomers (equal to the number of catenated rings). Their size, $\tilde{\sigma}$ was set by matching the mean-squared bond length of the effective chain, $\langle \tilde{b}^2\rangle$, with the mean-square length of mechanical bonds in the catenanes. The equivalent bending rigidity, $\tilde{\kappa}_b$ was set so that the mean squared gyration radius matched the catenanes' one. Equivalent diffusivities for the centers of mass of the two systems were obtained by setting the mass of the effective monomers respectively equal to the total mass of each ring, $\tilde{M} = 40M$ and by increasing by the same factor the effective friction coefficient, $\tilde{\zeta} = 40\zeta$. The kinetic mapping was verified a posteriori with the consistency of τ_{diff}, the self-diffusion times of the two systems, that is, the time required by the system's center of mass to cover a mean square distance equal to $\langle R_g^2\rangle$.

Specifically, the slowest Rouse modes, whose amplitudes deviate most from Gaussianity (see Figure S7), appear less orthogonal at $\kappa_b/\epsilon = 0$, when the catenane backbone is stiffer, than at $\kappa_b/\epsilon = 20$, see Figure S8. This observation bears analogies with the case of ordinary worm-like chains, where increasing corrections to the plain Rouse mode analysis are required for stiffer chains.[54]

Statics of Interacting Catenanes. Finally, we discuss the case of interacting catenanes, which we addressed by considering solutions of 27 catenanes with rings of m = 40 monomers and different rigidity in the $0.6 \le \kappa_b/\epsilon \le 20$ range. The box size, $L = 85\sigma$, was chosen to be about twice the largest size of isolated catenanes, $2R_g$, compare to Table 2, which ensure a good packing density without a significant incidence of catenanes' self-interactions across the periodic boundaries.

Table 2. Gyration Tensor Eigenvalues for Isolated and Interacting Catenanes[a]

	catenane in isolation			catenane in solution		
κ_b/ϵ	$\langle\lambda_1^2\rangle$	$\langle\lambda_2^2\rangle$	$\langle\lambda_3^2\rangle$	$\langle\lambda_1^2\rangle$	$\langle\lambda_2^2\rangle$	$\langle\lambda_3^2\rangle$
0.6	186.8	38.5	13.5	168.8	38.6	13.5
2	221.8	45.6	16.4	193.2	44.9	16.3
5	295.0	60.1	22.4	236.4	57.0	21.8
10	346.8	72.0	27.1	254.4	65.6	26.3
20	377.7	79.4	30.4	272.2	70.3	28.1

[a]Ranked eigenvalues of the gyration tensor of isolated and interacting catenanes made of rings with m = 40 beads and bending rigidity κ_b, as indicated. The eigenvalues are expressed in units of σ^2 and their statistical errors are about 2%. The interacting case corresponds to solutions of 27 catenanes in a periodic simulation box of side $L = 85\sigma$, as illustrated in Figure 8.

A typical equilibrated configuration of the system is shown in Figure 8a, where different chains are highlighted in different colors. Although the catenanes in the shown systems have the same number of rings, same ring length, and are packed at the same nominal density, the overlap of the catenanes varies noticeably with κ_b, see Figure 8b.

At a qualitative level, this is consistent with the κ_b-dependent size of isolated chains, which have a smaller metric footprint when the interlocked components are flexible. Quantitatively, we observe that at all κ_b's, the size of the catenanes is reduced by their interaction in solution. The result, which is consistent with the data of ref45 for fully flexible ring, holds at all rings rigidities. Figure 8c especially establishes that the size reduction is strongly modulated by the rings rigidity.

The effect is quantified in Table 2, which reports the principal components of the gyration tensor of isolated and interacting catenanes, and is illustrated in Figure 8c. The figure shows how κ_b affects the interacting catenanes gyration ellipsoid volume relative to the isolated case. One observes that while the changes are modest for flexible rings, they become very significant for rigid rings, where the effective volume is reduced by 50% compared to the isolated case. This indicates that, although the relative fluctuations of b are practically identical for isolated flexible and rigid rings, the latter endow catenanes with larger compressibility, which becomes manifest in crowded environments.

A further effects of crowding is to induce an orientational order of contacting rings in different catenanes. Figure 8d shows that at all κ_b's, there is a tendency for coplanarity of rings in close spatial proximity, similarly to columnar stacking.[55] The ordering effect is however lost at distances a few times larger than the rings gyration radius. On the contrary, the rings size and shape and the intrachain orientational order are practically unaffected by crowding at the considered density, see Figures S2−S4 and Table S1 for a direct comparison with the isolated case.

Dynamics of Interacting Catenanes. A natural question is how exactly the dynamics of interacting catenanes is affected by their κ_b-dependent metric footprint. Of particular interest is the mobility of catenanes, or diffusion coefficient, which could be measured experimentally, for example, by tracking fluorescently labeled catenanes.

We accordingly analyzed the mean squared displacement of the catenanes CoMs over timespans of $75 \times 10^3\tau_{LJ}$, which are long enough that the covered distances exceed the mean catenane size and catenanes separation. The results are given in Figure 8e and show that, at equal overall density, the mobility is slowest for catenanes with rigid rings. We conclude that, although the latter have the largest flexibility and compressibility, they form a more diffuse network of intercatenane topological constraints, which hinders their large-scale motion relative to flexible rings. In quantitative terms, the relative decrease of mobility from $\kappa_b = 0.6\epsilon$ to $\kappa_b = 20\epsilon$ is about 50%.

Detection of Catenanes Threadings. We finally considered the possibility that threadings among catenanes could occur in the crowded solutions, leading to long-lived entangled states. For all sampled configuration of the solutions we considered each catenane in turn and assessed whether its

https://doi.org/10.1021/acs.macromol.1c02542
Macromolecules XXXX, XXX, XXX−XXX

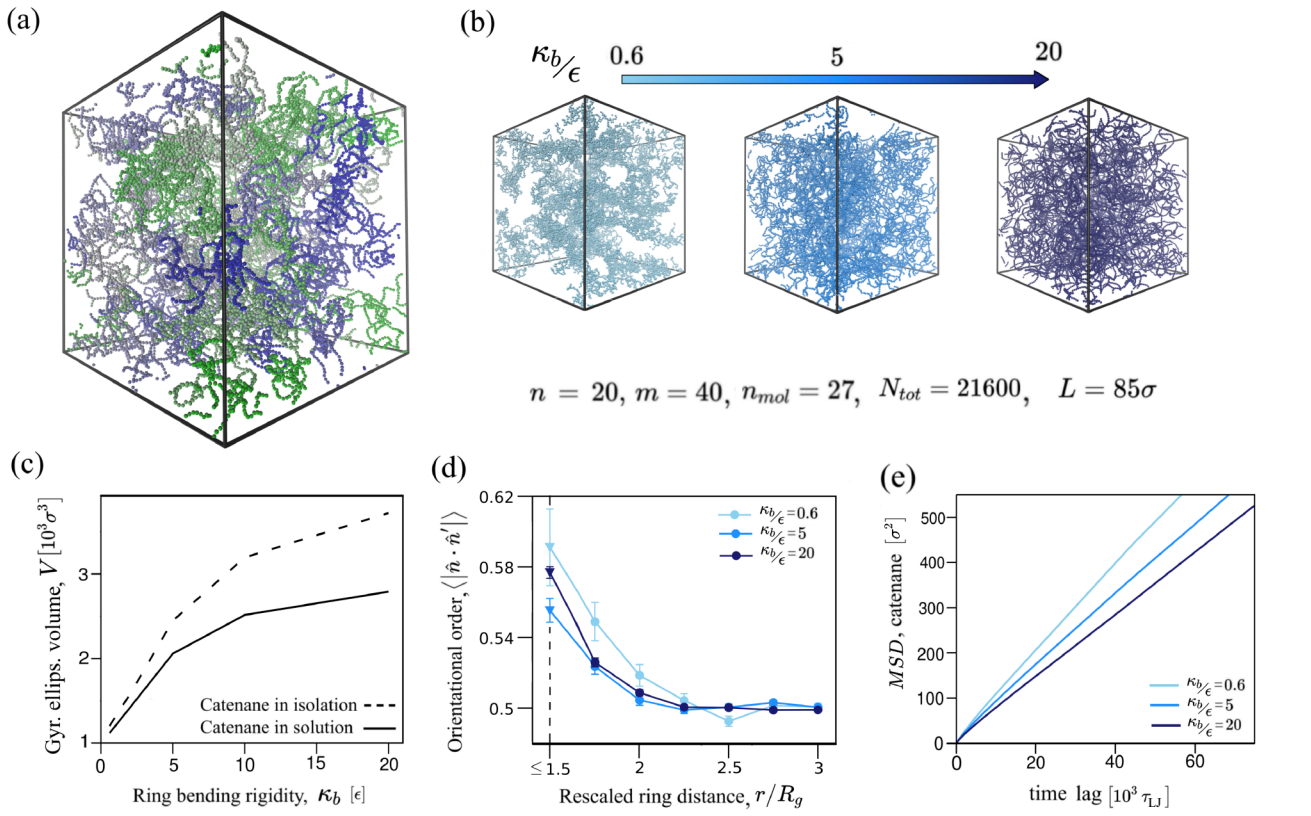

Figure 8. Effects of ring rigidity on the statics and dynamics of interacting catenanes. We considered solutions of n_{mol} = 27 catenanes, each consisting of n = 20 rings made of m = 40 monomers, packed inside a periodic simulation box of side $L = 85\sigma$. A typical configuration of the system for rings with rigidity $\kappa_b = 5\epsilon$ is shown in panel (a), where different colors are used for different catenanes. (b) Typical configurations at three different ring rigidities, as indicated. A uniform color was used to better convey the varying degree of catenane intermingling with κ_b. (c) κ_b-dependence of the average gyration ellipsoid volume, V, of catenanes in isolation and in solution. (d) Orientational order of rings in different catenanes as a function of their CoMs distance. To better highlight the role of steric interactions, the rings' distance was rescaled by the corresponding average gyration radius of catenated rings. (e) The κ_b-dependence of catenane mobility in solution is characterized via the mean squared distance (MSD) covered by the catenanes' centers of mass at different time lags.

backbone was physically linked[14,23] with nearby ring of other catenanes. As a measure of physical linking we considered the Gaussian integral.[14,16] The integral, which for closed curves yields the linking number, is expected to deviate significantly from 0 in case of threadings among the catenanes. No such outlier values were found among the about one hundred uncorrelated solution samples collected at each considered value of κ_b, see Figure S9. This indicates that catenanes threadings are rare at the considered conditions. However, such threadings ought to become more probable at larger crowding and/or with catenane length. We believe this point would be worthy of future investigations as threading probability could carry an interesting dependence on rings rigidity.

DISCUSSION AND CONCLUSIONS

We considered linear poly[n]catenanes, both isolated and in solution, and carried out the first systematic study of how the structural rigidity of the constitutive rings affects the statics and dynamics of these systems.

The main emergent property that we established is that increasing ring bending rigidity yields catenanes whose backbone is larger in size, but is also more flexible. We observed that the effect grows with the length of the rings. For the largest considered rings, made of m = 40 monomers, we found that the gyration radius of poly[20]catenanes increases by about 50% when going from fully flexible to rigid rings. Concomitantly, the effective persistence length of the catenanes backbone goes from 1.84 to 1.42 mechanical bonds, a 30% decrease.

The softening of the backbone is not caused by the larger wiggle room of stiffer concatenaned rings. In fact, the relative fluctuations of mechanical bond length are nearly identical for catenanes with flexible or rigid rings. Instead, by switching off excluded volume interactions of rings at different sequence separations, we established that the largest contribution to the catenane backbone rigidity is the steric hindrance of nearby rings. More specifically, it is the variation of ring shape from slightly prolate to oblate, that modulates the steric repulsion of the rings and ultimately the effective rigidity of the catenane.

Dynamical properties are shown to be strongly affected by increasing ring rigidity, too. In fact, a several-fold slowing down is systematically observed for very different processes, from segmental dynamics to Rouse modes relaxation, throughout the range of corresponding length scales.

Finally, we examined the implications of ring bending rigidity on the statics and dynamics of solutions of tens of catenanes packed at the same nominal density. Specifically, the packing density was set so that neighboring catenanes, with either rigid or flexible rings, were at a distance comparable to their size in isolation. We observed that crowding conditions

https://doi.org/10.1021/acs.macromol.1c02542
Macromolecules XXXX, XXX, XXX−XXX

cause a sizable shrinking in size of catenanes with rigid rings, which loose about a third of their gyration ellipsoid volume in isolation. Notwithstanding this crowding-induced size reduction, the metric footprint of catenanes with stiff rings remains larger than with flexible rings, with the consequences that the former offer a larger hindrance to each other's motion. In fact, we found that the diffusion coefficient of catenanes with rigid rings is 50% smaller than those with flexible ones.

The flexibility of interlocked components thus emerges as a key design element of supramolecular constructs to control their, flexibility, compressibility, internal dynamics, and mobility in crowded conditions. The observed effects on statics and dynamics could be harnessed for practical purposes, including sorting ones[56,57] to separate polydispersed solutions of catenanes with different ring rigidities or backbone topologies. Further theoretical and experimental perspectives could also be opened by systems where the rigidity of the interlocked components can be controlled externally, that is, by the binding of ligands or, for charged rings, by changing the ionic strength of the solution.

■ ASSOCIATED CONTENT

Supporting Information

The Supporting Information is available free of charge at https://pubs.acs.org/doi/10.1021/acs.macromol.1c02542.

Additional results for the size of backbone segments, ring size and shape, intrachain orientational order, catenane internal dynamics, and detection of threading events (PDF)

■ AUTHOR INFORMATION

Corresponding Author

Cristian Micheletti − *International School for Advanced Studies (SISSA), 34136 Trieste, Italy;* orcid.org/0000-0002-1022-1638; Email: cristian.micheletti@sissa.it

Author

Pietro Chiarantoni − *International School for Advanced Studies (SISSA), 34136 Trieste, Italy;* orcid.org/0000-0002-9249-863X

Complete contact information is available at: https://pubs.acs.org/10.1021/acs.macromol.1c02542

Notes

The authors declare no competing financial interest.

■ ACKNOWLEDGMENTS

We thank Phillip M. Rauscher for stimulating discussions.

■ REFERENCES

(1) Shapiro, T. A.; Englund, P. T. The structure and replication of kinetoplast DNA. *Annual review of microbiology* **1995**, *49*, 117−143.

(2) Arsuaga, J.; Blackstone, T.; Diao, Y.; Karadayi, E.; Saito, Y. Linking of Uniform Random Polygons in Confined Spaces. *J. Phys. A: Math. Gen.* **2007**, *40*, 1925−1936.

(3) Atapour, M.; Soteros, C.; Ernst, C.; Whittington, S. The linking probability for 2-component links which span a lattice tube. *J. Knot Theor. Ramif.* **2010**, *19*, 27−54.

(4) Niu, Z.; Gibson, H. W. Polycatenanes. *Chem. Rev.* **2009**, *109*, 6024−6046.

(5) Ayme, J.-F.; Beves, J. E.; Campbell, C. J.; Leigh, D. A. Template synthesis of molecular knots. *Chem. Soc. Rev.* **2013**, *42*, 1700−1712.

(6) Gil-Ramírez, G.; Leigh, D. A.; Stephens, A. J. Catenanes: Fifty Years of Molecular Links. *Angew. Chem., Int. Ed.* **2015**, *54*, 6110−6150.

(7) Erbas-Cakmak, S.; Leigh, D. A.; McTernan, C. T.; Nussbaumer, A. L. Artificial molecular machines. *Chem. Rev.* **2015**, *115*, 10081−10206.

(8) Piskadlo, E.; Oliveira, R. A. A topology-centric view on mitotic chromosome architecture. *International journal of molecular sciences* **2017**, *18*, 2751.

(9) Caraglio, M.; Orlandini, E.; Whittington, S. G. Driven Translocation of Linked Ring Polymers through a Pore. *Macromol.* **2017**, *50*, 9437−9444.

(10) Stolz, R.; Yoshida, M.; Brasher, R.; Flanner, M.; Ishihara, K.; Sherratt, D.; Shimokawa, K.; Vazquez, M. Pathways of DNA unlinking: A story of stepwise simplification. *Sci. Rep.* **2017**, *7*, 12420.

(11) Jiao, Y.; Stoddart, J. F. Weaving on the molecular scale. *Matter* **2021**, *4*, 2582−2584.

(12) Klotz, A. R.; Soh, B. W.; Doyle, P. S. Equilibrium structure and deformation response of 2D kinetoplast sheets. *Proc. Natl. Acad. Sci. U.S.A.* **2020**, *117*, 121−127.

(13) Caraglio, M.; Orlandini, E.; Whittington, S. G. Translocation of links through a pore: effects of link complexity and size. *J. Stat. Mech.: Theory and Exp.* **2020**, *2020*, 043203.

(14) Orlandini, E.; Micheletti, C. Topological and physical links in soft matter systems. *J. Phys.: Condens. Matter* **2022**, *34*, 013002.

(15) Dyson, S.; Segura, J.; Martínez-García, B.; Valdés, A.; Roca, J. Condensin minimizes topoisomerase II-mediated entanglements of DNA in vivo. *EMBO J.* **2021**, *40*, No. e105393.

(16) Baiesi, M.; Orlandini, E.; Trovato, A.; Seno, F. Linking in domain-swapped protein dimers. *Scient. Rep* **2016**, *6*, 33872.

(17) Dabrowski-Tumanski, P.; Sulkowska, J. I. Topological knots and links in proteins. *Proc. Natl. Acad. Sci. U. S. A.* **2017**, *114*, 3415−3420.

(18) Everaers, R.; Sukumaran, S. K.; Grest, G. S.; Svaneborg, C.; Sivasubramanian, A.; Kremer, K. Rheology and Microscopic Topology of Entangled Polymeric Liquids. *Science* **2004**, *303*, 823−826.

(19) Kremer, K.; Grest, G. S. Dynamics of entangled linear polymer melts: A molecular-dynamics simulation. *J. Chem. Phys.* **1990**, *92*, 5057−5086.

(20) Kalathi, J. T.; Kumar, S. K.; Rubinstein, M.; Grest, G. S. Rouse Mode Analysis of Chain Relaxation in Homopolymer Melts. *Macromolecules* **2014**, *47*, 6925−6931.

(21) Tzoumanekas, C.; Theodorou, D. N. Topological Analysis of Linear Polymer Melts: A Statistical Approach. *Macromolecules* **2006**, *39*, 4592−4604.

(22) Tzoumanekas, C.; Theodorou, D. N. From atomistic simulations to slip-link models of entangled polymer melts: Hierarchical strategies for the prediction of rheological properties. *Curr. Opin. Solid State Mater. Sci.* **2006**, *10*, 61−72.

(23) Caraglio, M.; Micheletti, C.; Orlandini, E. Physical Links: defining and detecting inter-chain entanglement. *Sci. Rep.* **2017**, *7*, 1156.

(24) Caraglio, M.; Micheletti, C.; Orlandini, E. Mechanical Pulling of Linked Ring Polymers: Elastic Response and Link Localisation. *Polymers* **2017**, *9*, 327.

(25) Liu, W.; Zhong, H.; Wang, R.; Seeman, N. C. Crystalline two-dimensional DNA-origami arrays. *Angew. Chem., Int. Ed.* **2011**, *50*, 264−267.

(26) Lee, J. B.; Peng, S.; Yang, D.; Roh, Y. H.; Funabashi, H.; Park, N.; Rice, E. J.; Chen, L.; Long, R.; Wu, M.; et al. A mechanical metamaterial made from a DNA hydrogel. *Nature Nanotechnol.* **2012**, *7*, 816−820.

(27) Polles, G.; Orlandini, E.; Micheletti, C. Optimal Self-Assembly of Linked Constructs and Catenanes via Spatial Confinement. *ACS Macro Lett.* **2016**, *5*, 931−935.

(28) Ding, T.; Yang, J.; Pan, V.; Zhao, N.; Lu, Z.; Ke, Y.; Zhang, C. DNA nanotechnology assisted nanopore-based analysis. *Nucleic acids research* **2020**, *48*, 2791−2806.

(29) August, D. P.; Dryfe, R. A.; Haigh, S. J.; Kent, P. R.; Leigh, D. A.; Lemonnier, J.-F.; Li, Z.; Muryn, C. A.; Palmer, L. I.; Song, Y.; et al. Self-assembly of a layered two-dimensional molecularly woven fabric. *Nature* **2020**, *588*, 429−435.
(30) Fairlamb, A. H.; Weislogel, P. O.; Hoeijmakers, J. H.; Borst, P. Isolation and characterization of kinetoplast DNA from bloodstream form of Trypanosoma brucei. *J. Cell Biol.* **1978**, *76*, 293−309.
(31) Chen, J.; Rauch, C. A.; White, J. H.; Englund, P. T.; Cozzarelli, N. R. The topology of the kinetoplast DNA network. *Cell* **1995**, *80*, 61−69.
(32) Soh, B. W.; Doyle, P. S. Deformation Response of Catenated DNA Networks in a Planar Elongational Field. *ACS Macro Lett.* **2020**, *9*, 944−949.
(33) Soh, B. W.; Doyle, P. S. Equilibrium Conformation of Catenated DNA Networks in Slitlike Confinement. *ACS Macro Lett.* **2021**, *10*, 880−885.
(34) Krajina, B. A.; Zhu, A.; Heilshorn, S. C.; Spakowitz, A. J. Active DNA Olympic Hydrogels Driven by Topoisomerase Activity. *Phys. Rev. Lett.* **2018**, *121*, 148001.
(35) Sakai, Y.; Wilkens, G. D.; Wolski, K.; Zapotoczny, S.; Heddle, J. G. Topogami: Topologically Linked DNA Origami. *ACS Nanoscience Au* **2022**, *2*, 57−63.
(36) Wasserman, E. The Preparation of Interlocking Rings: a Catenane1. *J. Am. Chem. Soc.* **1960**, *82*, 4433−4434.
(37) Dietrich-Buchecker, C. O.; Sauvage, J. P.; Kern, J. M. Templated synthesis of interlocked macrocyclic ligands: the catenands. *J. Am. Chem. Soc.* **1984**, *106*, 3043−3045.
(38) Chichak, K. S.; Cantrill, S. J.; Pease, A. R.; Chiu, S.-H.; Cave, G. W. V.; Atwood, J. L.; Stoddart, J. F. Molecular Borromean Rings. *Science* **2004**, *304*, 1308−1312.
(39) Leigh, D. A.; Pritchard, R. G.; Stephens, A. J. A Star of David catenane. *Nat. Chem.* **2014**, *6*, 978−982.
(40) Wu, Q.; Rauscher, P. M.; Lang, X.; Wojtecki, R. J.; de Pablo, J. J.; Hore, M. J. A.; Rowan, S. J. Poly[n]catenanes: Synthesis of molecular interlocked chains. *Science* **2017**, *358*, 1434−1439.
(41) Datta, S.; et al. Self-assembled poly-catenanes from supramolecular toroidal building blocks. *Nature* **2020**, *583*, 400−405.
(42) Collier, C. P.; Mattersteig, G.; Wong, E. W.; Luo, Y.; Beverly, K.; Sampaio, J.; Raymo, F. M.; Stoddart, J. F.; Heath, J. R. A [2]Catenane-Based Solid State Electronically Reconfigurable Switch. *Science* **2000**, *289*, 1172−1175.
(43) Hart, L. F.; Hertzog, J. E.; Rauscher, P. M.; Rawe, B. W.; Tranquilli, M. M.; Rowan, S. J. Material properties and applications of mechanically interlocked polymers. *Nature Reviews Materials* **2021**, *6*, 508−530.
(44) Rauscher, P. M.; Rowan, S. J.; de Pablo, J. J. Topological Effects in Isolated Poly[n]catenanes: Molecular Dynamics Simulations and Rouse Mode Analysis. *ACS Macro Lett.* **2018**, *7*, 938−943.
(45) Rauscher, P. M.; Schweizer, K. S.; Rowan, S. J.; de Pablo, J. J. Thermodynamics and Structure of Poly[n]catenane Melts. *Macromolecules* **2020**, *53*, 3390−3408.
(46) Rauscher, P. M.; Schweizer, K. S.; Rowan, S. J.; de Pablo, J. J. Dynamics of poly[n]catenane melts. *J. Chem. Phys.* **2020**, *152*, 214901.
(47) Ahmadian Dehaghani, Z.; Chubak, I.; Likos, C. N.; Ejtehadi, M. R. Effects of topological constraints on linked ring polymers in solvents of varying quality. *Soft Matter* **2020**, *16*, 3029−3038.
(48) Lei, H.; Zhang, J.; Wang, L.; Zhang, G. Dimensional and shape properties of a single linear polycatenane: Effect of catenation topology. *Polymer* **2021**, *212*, 123160.
(49) Li, J.; Gu, F.; Yao, N.; Wang, H.; Liao, Q. Double Asymptotic Structures of Topologically Interlocked Molecules. *ACS Macro Lett.* **2021**, *10*, 1094−1098.
(50) Plimpton, S. Fast parallel algorithms for short-range molecular dynamics. *J. Comput. Phys.* **1995**, *117*, 1−19.
(51) Alim, K.; Frey, E. Shapes of Semiflexible Polymer Rings. *Phys. Rev. Lett.* **2007**, *99*, 198102.
(52) Doi, M.; Edwards, S. F.; Edwards, S. F. *The Theory of Polymer Dynamics*; Oxford University Press: Oxford, 1988; Vol. 73.
(53) Paul, W.; Smith, G. D.; Yoon, D. Y. Static and Dynamic Properties of a n-C100H202 Melt from Molecular Dynamics Simulations. *Macromolecules* **1997**, *30*, 7772−7780.
(54) Groot, R. D. Mesoscale simulation of semiflexible chains. I. Endpoint distribution and chain dynamics. *J. Chem. Phys.* **2013**, *138*, 224903.
(55) Poier, P.; Bačová, P.; Moreno, A. J.; Likos, C. N.; Blaak, R. Anisotropic effective interactions and stack formation in mixtures of semiflexible ring polymers. *Soft Matter* **2016**, *12*, 4805−4820.
(56) Weiss, L. B.; Marenda, M.; Micheletti, C.; Likos, C. N. Hydrodynamics and Filtering of Knotted Ring Polymers in Nanochannels. *Macromolecules* **2019**, *52*, 4111−4119.
(57) Marenda, M.; Orlandini, E.; Micheletti, C. Sorting ring polymers by knot type with modulated nanochannels. *Soft Matter* **2017**, *13*, 795−802.

https://doi.org/10.1021/acs.macromol.1c02542
Macromolecules XXXX, XXX, XXX−XXX